Measurement Report: Rapid changes of chemical characteristics and health risks for high time-resolved trace elements in $PM_{2.5}$ in a typical industrial city in response to stringent clean air actions

Rui Li[a *], Yining Gao[a], Yubao Chen[a], Meng Peng[b c *], Weidong Zhao[c *], Gehui Wang[a], Jiming Hao[b]

[a] *Key Laboratory of Geographic Information Science of the Ministry of Education, School of Geographic Sciences, East China Normal University, Shanghai, 200241, PR China*

[b] *State Key Joint Laboratory of Environment Simulation and Pollution Control, School of Environment, Tsinghua University, Beijing, 100084, P.R. China*

[c] *Institute of energy conservation and environmental protection, China Electronic Information Industry Development Research Institute, Beijing, 100084, P.R. China*

*** Correspondence to:**

Prof. Li (rli@geo.ecnu.edu.cn), Dr. Peng (mvponesky@163.com), and Prof. Zhao (zhaoweidong@ccidthinktank.com)

Abstract

Atmospheric trace metals entail significant damages in human health and ecosystem safety, and thus a series of clean air actions have been implemented to decrease the ambient element concentrations. Unfortunately, the impact of these emission control measures on element concentrations in fine particles remained poorly understood. In our study, the random forest (RF) model was applied to distinguish the effects of emission and meteorology to trace elements in $PM_{2.5}$ in a typical industrial city named Tangshan based on a three-year (2017-2020) hourly field observation. The result suggested that the clean air actions have facilitated the dramatic decreases of the deweathered concentrations of Ga, Co, Pb, Zn, and As by 72%, 67%, 62%, 59%, and 54%, respectively. It is attributable to the strict implementation of "coal to gas" strategies and optimization of industrial structure and layout. However, the deweathered levels of Ca (8.3%), Cr (18.5%), and Fe (23%) only displayed minor decreases, indicating that the emission control measures for ferrous metal smelting and vehicle emission were not very effective. The positive matrix factorization (PMF) results suggested that the contribution ratios of biomass burning, non-

ferrous metal smelting, coal combustion, ferrous metal smelting, heavy oil combustion, and traffic-related dust changed from 33%, 11%, 15%, 13%, 3%, and 25% to 33%, 8%, 8%, 13%, 4%, and 33%, respectively. To date, no significant noncarcinogenic and carcinogenic risks were observed for all of the elements, while both of As and Pb still showed relatively high health damages. It was proposed to further cut down the combustion-related emissions (e.g., As and Pb) because it showed the highest marginal health benefits. Besides, the control of traffic-related emissions might be a key abatement strategy to facilitate the reduction of elements in fine particles.

Keywords: hourly trace elements; chemical characteristics; health risks; clean air actions; Tangshan

1. Introduction

Along with the rapid economic development and accelerated urbanization, the energy consumption and output of various industrial products worldwide displayed the persistent increases, thereby leading to the massive emissions of elements especially trace metals into the atmosphere (Tian et al., 2015; Zhu et al., 2020). These elements injected into the atmosphere could pose great threaten to the terrestrial and aquatic ecosystem via dry/wet deposition and then endanger human health through the physiochemical transfer and bioaccumulation in food chains (Fernandez et al., 2000; Harmens et al., 2010; Storelli, 2008). For instance, some toxic trace metals including cadmium (Cd), lead (Pb), and mercury (Hg) were often regarded as human carcinogens even in trace amounts (Micheline et al., 2019; Olujimi et al., 2015). Besides, the excessive accumulation of some biological essential elements such as copper (Cu), iron (Fe), and zinc (Zn) could initiate activation of inflammatory cascades in tissues and the induction of biochemical synthesis pathways by catalyzing the generation of reactive oxygen species (ROS) (Alies et al., 2013; Lopez-Cruz et al., 2016; Saffari et al., 2014), though minor enrichment of these elements was beneficial to the human health and plant growth (Oldani et al., 2017). Apart from the health impacts, some transition metals (e.g., Ni, Zn) could catalyze some chemical reactions such as particle-phase sulfate generation and heterogeneous production and removal of gas-phase hydrogen oxide radicals (HO_x) to aggravate the haze formation (Clements et al., 2013; Guo et al., 2014). Therefore, it is highly imperative to recognize the pollution status of elements in the atmosphere, to identify the major sources and then to propose effective controls measures to alleviate their negative effects on air pollution and human health especially in some developing countries.

In the past decades, hundreds of studies investigated the pollution levels of elements and revealed their sources in various study regions including urban (Das et al., 2018; Duan and Tan, 2013; Lyu et al., 2017; Grivas et al., 2018; Clements et al., 2014), marine (Shi et al., 2015; Witt et al., 2006), mountain (Kang et al., 2016). Most of these studies used the filter sampling (one sample or two samples each day) technique coupled with offline analysis using inductively coupled plasma mass spectrometry (ICP-MS) or inductively coupled plasma-atomic emission spectrometry (ICP-AES) to determine the element concentrations in the atmosphere (Ao et al., 2019; Lin et al., 2016). Although these studies have obtained many valuable information about the occurrence levels and key sources of ambient elements, the low time-resolution data cannot accurately reflect the dynamic transformation and evolution of ambient elements. It was well known that atmospheric emissions, transport and deposition significantly relied on rapidly evolving meteorological conditions (Holden et al., 2016; Rasmussen, 1998), and thus the offline samples inevitably ignored the impacts of environmental shifts with rapid temporality on the atmospheric element concentrations. Moreover, most of current source apportionment studies employed the receptor models (positive matrix factorization (PMF)) to determine the potential sources of elements (Jeong et al., 2016; Lyu et al., 2017), and the accuracy of these models was strongly dependent on the sample size and time resolution (Liu et al., 2018b). In this regard, the high time-resolved observation of atmospheric elements provided an unprecedented opportunity to characterize the occurrence levels, identify their major sources, and assess the health impacts.

To date, only a few studies applied the high-resolution devices to capture the hourly variability of ambient elements. Prati et al. (2000) firstly used Particle Induced X-ray Emission (PIXE) measurements to analyze hourly trace elements in Genoa in Italy. Following this work, A. D'Alessandro et al. (2003) and Dall'Osto et al. (2013) also employed the same technique to determine the trace metals in Italian towns and Barcelona, respectively. Later on, Jeong et al. (2016) used Xact metals monitor to reveal the temporal variability of atmospheric elements in Toronto, Canada in summer and winter during 2013-2014. Recently, the Xact metals monitor has begun to be performed in China due to the higher accuracy and convenience. Chang et al. (2018) firstly used the online multi-element analyzer to achieve a one-year near real-time observation of ambient elements in China and found traffic, nonferrous metal smelting and coal combustion were major

sources of atmospheric trace metals. Afterwards, Cui et al. (2019) applied the analyzer to monitor 1-year atmospheric elements, and demonstrated that dust, industry, and biomass burning were considered as the dominant sources of most trace elements in Beijing, accounting for 36%, 10.7%, and 27% of total $PM_{2.5}$ concentration, respectively. Up to date, continuous hourly element observation was only performed less than one year in most of the previous studies, and the long-term temporal variability of absolute concentrations and key pollution sources of atmospheric elements cannot be fully revealed.

Since 2013, Chinese government proposed strict Air Pollution Prevention and Control Action Plan (the Action Plan) across China and the emissions of multiple gaseous pollutants suffered from significant decreases. In turn, the absolute concentrations and health effects of air pollutants also experienced the rapid changes response to these stringent control measures. Zhang et al. (2019) reported that the population-weighted annual mean $PM_{2.5}$ concentration decreased from 62 to 42 $\mu g/m^3$ during 2013-2017 and reduced $PM_{2.5}$-attributable premature deaths by 0.4 million due to the impact of the Action Plan. Shortly after that, Geng et al. (2019) estimated that the population-weighted mean concentrations of SO_4^{2-}, NO_3^-, and NH_4^+ in $PM_{2.5}$ decreased from 11.1, 13.8, and 7.4 $\mu g/m^3$ to 6.7, 13.1, and 5.8 $\mu g/m^3$, respectively during the same period. Nevertheless, the impact of the Action Plan on trace elements in fine particles still remained poorly understood. Especially, the knowledge about the variation of source apportionment and health risks for trace elements response to the Action Plan was extremely limited. Moreover, most of the previous studies only utilized the original concentrations to analyze the impact of clean air policy (He et al., 2021; Xiao et al., 2020). It was well known that the pollutant concentrations in the atmosphere were affected by meteorology and anthropogenic emissions simultaneously (Li et al., 2021), and the use of original element concentrations alone cannot assess the unique contribution of emission reduction to the air pollutants. Thus, it is urgently needed to remove the effect of meteorology and accurately capture the independent influence of the Action Plan on the chemical characteristics, source apportionment, and health risks of trace elements. Such knowledge is critical to design effective air pollution mitigation strategies in the near future.

As a heavily industrialized city located in North China Plain (NCP), Tangshan possesses many energy-intensive industries including coal-fired power plants, non-ferrous smelting industries,

textiles, building materials, chemical engineering, and papermaking industries (Ren et al., 2011). Intensifying industrial development and urbanization aggravated local air quality. Previous studies performed in Tangshan focused on the trace metals in soils and dusts (Cui et al., 2020; Song et al., 2011), whereas no study analyzed the long-term and high-resolution variabilities of atmospheric elements. Since 2013, many emission control measures such as the establishment of desulfurization and denitration facilities for coal-fired power sector have been strictly implemented in Tangshan (Ma et al., 2019). Especially after 2017, coal to gas project has started to be implemented in Tangshan and the energy structure suffered from significant change (Wang et al., 2020b). In response to substantial pollution control policies, the chemical compositions and major sources of trace elements might show corresponding change. Here, we conducted a near real-time measurement of atmospheric elements in $PM_{2.5}$ using a Xact multi-metals analyzer in Tangshan, China during September 2017 to August 2020. The primary objectives of our study were to (1) determine the occurrence levels of elements in $PM_{2.5}$ of Tangshan; (2) to analyze the seasonal and intra-week variations of atmospheric elements and to distinguish the separate contributions of emission and meteorology to these species; (3) to quantify the changes of major sources for atmospheric elements during this period; (4) to assess the changes of health risks in response to these pollution control measures.

2. Material and methods

2.1 Sampling site

The sampling site (39.66°N, 118.18°E) is situated on the rooftop (~20 m above the ground) of a building in the urban district of Tangshan and no high buildings spread around within 100 m range. The sampling site is close to some major roads including Airport Road, Huayan North Road, and Changhong Road. A large number of commercial streets and recreation facility surround the site. Although no big industrial point source was closely adjacent to the sampling site, many potential pollution sources were located more than 15 km away from the site. For instance, Beihu industrial region is located about 15 km in the eastern direction of the site. Some large iron steel industries and nonferrous/ferrous smelting industries were located on the north of sampling site (more than 30 km). Besides, most of large petrochemical industries, coal-fired power plants, and shipping industries focus on Caofeidian and Haigang developing zones, both of which were located about 50

144 km in the South area of the sampling site. The detailed location is depicted in Figure 1.

145 2.2 Instrumentation

146 Hourly mass concentrations of 22 elements, including Ag, As, Au, Ca, Co, Cu, Cd, Cr, Fe, Ga,
147 Hg, K, Mn, Ni, Pb, Pd, Sb, Se, Sn, Tl, V, and Zn in $PM_{2.5}$ were determined by an online multi-
148 element analyzer (Model Xact 625, Cooper Environment Service, USA) (Table S1). The sample air
149 is drawn through a small spot on the tape where the $PM_{2.5}$ was collected at a flow rate of 16.7 L
150 min^{-1} during September 2017-August 2020. An internal Pd pod is utilized as an internal standard to
151 detect the stability of the instrument. Tl was removed from the datasets because over 95% of their
152 concentrations were below the limit of detection (LOD) (Table S2). Au, Cd, Sn and Sb were also
153 excluded from the datasets because over 50% of the concentrations for these metals were below the
154 LOD. To validate the reliability of online multi-element analyzer, many previous studies used the
155 filter sampling coupled with ICP-MS and ICP-AES to determine the daily concentrations of
156 elements and confirmed that the online device showed good agreement with the filter sampling
157 (Furger et al., 2017; Tianxue et al., 2006). Hourly averaged meteorological parameters including air
158 temperature (T), relative humidity (RH), air pressure (P), wind direction (WD), and wind speed
159 (WS) during the sampling period were measured by a weather station with sonic anemometer
160 (150WX, Airmar, Milford, NH, USA). The hourly mass concentration of $PM_{2.5}$ was determined by
161 the particulate monitor (Thermo, FH62C-14). The routine procedures, including the daily zero or
162 standard calibration, span and range check, station environmental control and staff certification,
163 followed the Technical Guideline of Automatic Stations of Ambient Air Quality in Tangshan based
164 on the national specification HJ/T193-2005, which was revised based on the technical guidance
165 established by the US EPA. Quality Assurance and Quality Control (QA/QC) for the Xact
166 measurements was implemented throughout the sampling period. The internal Pd upscale value was
167 recorded after daily programmed test for the instrument.

168 2.3 Deweathered model development

169 The concentrations of air pollutants were affected by meteorological parameters and emissions
170 simultaneously. In order to separate the contributions of emissions, the impacts of meteorological
171 conditions must be eliminated. In this study, a typical machine-learning model named random forest
172 (RF) approach was applied to distinguish the effects of emissions and meteorological conditions

(Chen et al., 2018). All of trace elements in $PM_{2.5}$ were treated as the dependent variables. The time predictors (year, day of year (DOY), day of week (DOW), hour of day (HOY)) and meteorological factors including air temperature (T), relative humidity (RH), wind speed (WS), wind direction (WD), and air pressure (P) were regarded as the predictors (Figure S1). The original dataset was randomly classified into a training dataset (80% of input dataset) for developing the RF model and the remained one was treated as the test dataset. After the building of the RF model, the deweathered technique was employed to predict the concentrations of trace elements at a specific time point. The deweathered element concentrations served as the concentrations contributed by emission alone. The differences of original element concentrations and deweathered element concentrations were regarded as the concentrations contributed by meteorology. Many statistical indicators including R^2 value, root-mean-square error (RMSE), and mean absolute error (MAE) were regarded as the major indicators to evaluate the RF modelling accuracy. The RF model with the 5-fold cross-validation R^2 value less than 0.5 was considered to be the unconvincing result and cannot reflect the impacts of emission and meteorology on air pollutants accurately because more than 50% variability of the training model cannot be appropriately explained. After the model evaluation, only the trace elements with the cross-validation R^2 values larger than 0.5 were selected to estimate the respective contributions of emission and meteorology to the total element concentrations.

2.4 PMF model

As a typical receptor model applied to source apportionment, PMF 5.0 version was used to identify the major origins of atmospheric elements and to determine the contribution ratio of each source to these elements. The objective of PMF is to solve the issues of chemical mass balance between measured concentration of each element and its source contributions by decomposing the input matrix into factor contribution and factor profile. The detailed equation is shown in Eq. (1). Besides, the contribution of each source for individual element must be non-negative because no sample has a negative source contribution. In brief, the basic principle of PMF is to calculate the least object function Q when the g_{ik} must be a positive-definite matrix based on Eq. (2) (Paatero and Tapper, 1994; Reff et al., 2007).

$$x_{ij} = \sum_{k=1}^{p} g_{ik} f_{kj} + e_{ij} \quad (1)$$

$$Q = \sum_{i=1}^{n}\sum_{j=1}^{m}\left[\frac{x_{ij} - \sum_{k=1}^{p} g_{ik} f_{kj}}{u_{ij}}\right]^2 \quad (2)$$

where x_{ij} and e_{ij} denote the concentration and uncertainty of jth element, respectively. g_{ik} represents the contribution ratio of kth source to ith sample, f_{kj} represents the ratio of jth element in kth source, and e_{ij} indicates the residual of jth element in the i sample. The uncertainties associated with factor profiles were evaluated using three error calculation methods including bootstraps (BS) method, displacement (DISP) analysis, and the combination method of DISP and BS (BS-DISP). For the BS method, 100 runs were performed and the result has been believed to be valid since all of the factors showed a mapping of above 90%. DISP analysis also confirmed that the solution was considered to be stable because the observed drop in the Q value was less than 0.1% and no factor swap occurred. For the BS-DISP analysis, the solution has been verified to be useful because the observed drop in the Q value was less than 0.5%. Furthermore, both of the results from BS and BS-DISP did not suggest any asymmetry or rotational ambiguity for all of the factors (Manousakas et al., 2017; Taghvaee et al., 2018).

2.5 Health risk assessment of trace metals in $PM_{2.5}$

As a typical industrial city, Tangshan possesses a large number of residents and poor air quality. Therefore, the residents in Tangshan might suffer from severe exposure risks of trace metals. In our work, the carcinogenic and non-carcinogenic risks of trace metals in $PM_{2.5}$ were evaluated based on some statistical threshold proposed by International Agency for Research on Cancer (IARC). Based on the criterion of IARC, As, Ni, Cr, and Pb were considered to be carcinogenic to humans.

The carcinogenic and non-carcinogenic risks induced by meatal exposure for adults and children were evaluated based on the carcinogenic risks (CR) and hazard quotient (HQ). The formulas for calculating ADD, CR, and HQ are as follows:

$$ADD=(C\times InhR\times EF\times ED)/(BW\times AT) \quad (3)$$

$$HQ=ADD/RfD \quad (4)$$

$$CR = ADD\times CSF \quad (5)$$

where C (mg m^{-3}) denotes the concentration of the corresponding trace metal in $PM_{2.5}$; InhR is the respiratory rate; EF represents the annual exposure frequency (d y^{-1}); ED is the exposure duration; BW is the average body weight; AT denotes the average exposure time; ADD means the daily intake

(mg/kg/day) of trace metals; RfD represents the reference dose, calculated with reference concentrations; CSF is the cancer slope factor. The potential non-carcinogenic risk of the trace metal might be high when HQ was above 1.0, whereas the health risk is not obvious when HQ is below 1.0. The carcinogenic risk of each trace metal is evaluated based on whether CR is higher than 10^{-4}.

3. Results and discussion

3.1 Occurrence levels and inter-annual variations of original element concentrations

The total mass concentrations of 16 elements in $PM_{2.5}$ of Tangshan varied between 230 ng/m^3 to 20000 ng/m^3, with the median value of 3100 ± 900 ng/m^3. The total element concentrations in Tangshan accounted for 5.7% of the total mass concentrations of $PM_{2.5}$, which was slightly higher than those in Beijing (4.7%) and Qingdao (4.0%), and significantly higher than that in Shanghai (1.80%) (Chang et al., 2018; Cui et al., 2019). As depicted in Figure 2, the concentrations of these elements followed the order of K (1400 ± 950 ng/m^3) > Fe (880 ± 590 ng/m^3) > Ca (330 ± 270 ng/m^3) > Zn (320 ± 160 ng/m^3) > Pb (58 ± 36 ng/m^3) > Mn (54 ± 32 ng/m^3) > Cu (22 ± 19 ng/m^3) > As (15.3 ± 11.0 ng/m^3) > Se (6.5 ± 5.3 ng/m^3) > V (4.0 ± 3.6 ng/m^3) > Cr (2.8 ± 2.2 ng/m^3) > Ag (2.8 ± 2.1 ng/m^3) > Ni (2.2 ± 1.8 ng/m^3) > Hg (1.5 ± 0.8 ng/m^3) > Ga (0.9 ± 0.7 ng/m^3) > Co (0.7 ± 0.2 ng/m^3). Among all of these elements, K, Fe, Zn, and Ca were most abundant species, accounting for 95% of the total elements in $PM_{2.5}$. The remaining element concentrations only accounted for less than 6% of the total element concentrations, which was similar to the previous studies (Chang et al., 2018; Cui et al., 2019). Nearly all of the trace elements in Tangshan, Beijing, Qingdao, and Shanghai were significantly lower than those in Zibo during 2006-2007 (Table S3). It suggested that the trace elements in China experienced marked decreases in the past decades (Zhang et al., 2018). Compared with some cities in some developed countries, all of the trace element concentrations were significantly higher than those in London and Toronto. However, the concentrations of K, Ca, V, Cr, Mn, and Fe in Tangshan were higher than those in Venice, Italy.

Due to the higher exposure risk and great threaten to human health, it is necessary to compare the trace metal concentrations with the risk threshold proposed by many organizations or countries. As shown in Table 1, we have collected many risk thresholds in different countries and found that the Hg (1.5 ± 0.8 ng/m^3), Ni (2.2 ± 1.8 ng/m^3), and Pb concentrations (58 ± 36 ng/m^3) in Tangshan

were significantly lower than the thresholds of the Chinese Ambient Air Quality Standard (CAAQS) (Hg: 50 ng/m^3), World Health Organization (WHO) (Hg: 1000 ng/m^3, Ni: 25 ng/m^3, and Pb: 1000 ng/m^3), Europe Union (EU) (Ni: 20 ng/m^3), and the United States (Pb: 150 ng/m^3). However, both of the As (15 ± 11 ng/m^3) and Cr concentrations (2.8 ± 2.2 ng/m^3) in $PM_{2.5}$ of Tangshan were much higher than the standard values of CAAQS (As: 6.0 ng/m^3 and Cr: 0.03 ng/m^3), WHO (As: 6.6 ng/m^3 and Cr: 0.25 ng/m^3), and EU (As: 6.0 ng/m^3).

The inter-annual variation of original concentrations of trace elements in $PM_{2.5}$ are depicted in Figure 3 and S2-S3. The original concentrations of all the trace elements exhibited the decreasing trends. Cu, Co, Zn, Pb, As, and Ga concentrations suffered from dramatic decreases from 37 to 12 ng/m^3 (68%), 1.21 to 0.4 ng/m^3 (66%), 400 to 190 ng/m^3 (53%), 71 to 40 ng/m^3 (44%), 20 to 11 ng/m^3 (44%), and 1.09 to 0.6 ng/m^3 (42%), respectively. Following these species, observed K (40%), Ag (39%), V (39%), Ni (36%), Ca (33%), Mn (29%), Se (29%), Fe (27%), and Cr (21%) concentrations showed moderate decreasing ratios. The observed Hg level exhibited the lowest decreasing ratio from 1.59 to 1.43 ng/m^3 (9.9%).

3.2 Impact of emission reduction on trace element concentrations

Although the original concentrations of trace elements could be utilized to analyze the impact of the clean air policy, the role of emission reduction on element concentration might not be clearly clarified because the meteorological factors were also important variables affecting the air quality. In order to accurately reflect the response of element concentrations to emission reduction alone during 2017-2020, the meteorological conditions were eliminated by RF model in our study. Based on the results in Figure S4, the RF models for all of the species showed better performance because their R^2 values were higher than 0.50, and the slopes of all of the fitting curves were also close to the R^2 values. The result suggested that the separation of meteorology and emission of trace elements based on RF model was reliable. During 2017-2020, the deweathered concentrations of Ga, Co, Pb, Zn, and As showed the rapid decreases from 1.52 to 0.4 ng/m^3 (72%), 1.31 to 0.4 ng/m^3 (67%), 92 to 35 ng/m^3 (62%), 410 to 170 ng/m^3 (59%), and 21 to 10 ng/m^3 (54%), respectively (Figure 3). It was well known that As, Co, and Pb were typical marker elements for coal combustion and the “coal-to-gas” and “coal-to-electricity” strategies have been widely performed in Tangshan (Fang et al., 2020; Li et al., 2017). Wang et al. (2020a) has estimated that these effective control

measures have contributed to around 60% of the total $PM_{2.5}$ reductions. Meanwhile, the upgradation and optimization of industrial structure/layout and the shutdown of high-pollution industries were also strictly implemented in Tangshan, and thus led to the dramatic decreases of Ga and Zn concentrations because Ga and Zn were common forms of nonferrous metal smelting (Tian et al., 2015). However, the deweathered Ca level displayed the lowest decrease ratio (8.3%) from 2017 to 2020, indicating that clean air actions cannot significantly reduce the fugitive emissions. In addition, the deweathered Fe (23%) and Cr (18.5%) also suffered from relatively low decrease ratios. It was well documented that Fe and Cr originated from metallurgical industry such as steel production and ferrous metal smelting (Tian et al., 2015), and the slight decreases of deweathered Fe and Cr levels during the sampling period suggested that the emission control measures for ferrous metal smelting should be strengthened in the future work.

In addition, the decreasing ratios of the deweathered concentrations for each species displayed different seasonal characteristics. The deweathered concentrations of some elements related with industrial activities (e.g., Ga, Zn, and Cr) suffered from rapid decreases in autumn and winter compared with other seasons during 2017-2020 (Figure 4), indicating that the optimization of industrial layout and shutdown of outdated industries were effective to decrease these element emissions especially in high-pollution season. Some elements derived from biomass burning including K (66%) and Se (50%) also suffered from the most dramatic decreasing ratios in autumn. It was assumed that enhanced crop residual burning occurred frequently during the autumn harvest season. Ke et al. (2019) confirmed that the number of fire spots in October-November was even higher than that in June and the burned area in harvest season was highest during 2013-2017. However, the control on open biomass burning has been implemented strictly in recent years, largely reducing the K and Se emissions in autumn. It should be noted that the deweathered Pb (46%), Co (65%), and As (45%) concentrations in winter did not display high decreasing ratios though the annual mean deweathered Pb, Co and As levels experienced dramatic decreases. The result revealed that it was still difficult to reduce the Pb, Co, and As emissions during the heating season because increased coal consumption for domestic heating largely offset the contributions of emission control measures (Zhu et al., 2018; Zhu et al., 2020).

Apart from the seasonal difference of each species, the decreasing ratios of these elements also

suffered from distinctly intra-weekly variations. The deweathered concentrations of most elements except Ca, Cu, Ni, and V exhibited the higher decreasing ratios at the weekends than those in the weekdays (Figure 5). Cui et al. (2020) has demonstrated that the weaker supervision on industrial enterprises on weekends could lead to the higher concentrations of non-traffic elements such as K, As, Se, and Cr in some cities. Fortunately, grid monitoring has been widely performed in Tangshan recently (http://hbepb.hebei.gov.cn/hbhjt/xwzx/jicengfengcai/101624062321621.html), and many low-cost sensors were installed at some energy-intensive industries, which could decrease the stealing emissions of some elements. Nonetheless, the decreasing ratios of Ca, Cu, V, and Ni did not show the regular intra-weekly characteristics. In recent years, Tangshan adopted strict traffic management regulation and the nonlocal light duty vehicles were restricted to drive inside the urban area one day per week based on the end number of the license plates (Westerdahl et al., 2009; Wu et al., 2011), whereas the restrictions were not valid at weekends (Liu et al., 2007). Theoretically, the traffic control should result in marked decreases of traffic-related element concentrations on weekdays compared with weekends. However, in our study, some traffic-related elements such as Ca and Cu did not show similar characteristics. Meanwhile, as the important tracer of vehicle emission, the NO_x concentration in Tangshan did not show regular intra-weekly pattern. It was supposed that the vehicle volume in Tangshan has increase from 2.0 to 2.4 million (http://tjj.hebei.gov.cn/), which largely offset the benefits of traffic controls. The shipping-related elements including Vi and Ni also did not show regular intra-weekly variation because no heavy metal emission control measures for shipping were performed.

3.3 The role of meteorology on the year-to-year variations of element concentrations

The difference of original and deweathered element concentrations could be regarded as the concentrations contributed by meteorological parameters. The positive impacts of meteorological parameters on trace elements suggested that the meteorological conditions were unfavorable to the pollutant diffusion, while the negative impacts of meteorological indicators meant the favorable condition to trace elements. In our study, the roles of meteorological conditions on Ca (-25%), V (-10%), Cr (-2.5%), Mn (-0.7%), Fe (-4.6%), Ni (-7.6%), and Cu (-21%) during 2017-2020 were negative (Figure S5), while the roles of meteorological parameters on other elements were positive. The result suggested that those elements derived from vehicle emission (Ca, Cu, and Fe), ferrous

metal smelting (Cr and Mn), and heavy oil combustion (V and Ni) were less sensitive to the emission reduction actions compared with other elements and the meteorological conditions were much beneficial to the diffusion of these elements. In order to further reveal the key meteorological factors for these elements, we used RF model to calculate the variable importance of all of these meteorological parameters including P, RH, T, WD, and WS. The result suggested that Ca, Fe, and Cu were mainly influenced by T, whereas V, Ni, Cr, and Mn were often associated with WD and WS (Figure 6). During the spring and summer in 2017-2020, the average air temperature decreased from 8.9 and 27 to 7.2 and 26°C, respectively. The decreased air temperature led to the higher water content in the soil and a lower tendency of dust suspension, and might decrease the concentrations of Ca, Fe, and Cu (Manju et al., 2018; Yang et al., 2017; Lyu et al., 2016). Although the annual average wind speed in Tangshan decreased from 1.70 to 1.45 m/s, the mean wind speed from the southeastern direction displayed slight increase from 1.34 to 1.50 m/s. Zhao et al. (2013) verified that V and Ni were usually emitted from heavy oil combustion of ocean-going ship engines. Many coastal ports and ferrous metal smelting industries were located on the southeastern direction of the sampling site, and thus the enhanced WS might promote the dilution and dispersion of trace elements (Figure S6-8). As shown in Figure S8, both of V and Ni showed the higher concentrations in the southeastern part of Tangshan and the concentrations displayed gradual decreases along the Southeast-Northwest transect, which also demonstrated that both of V and Ni in the sampling site could be derived from coastal shipping emission.

3.4 The impact of clean air policy on source apportionment of trace elements

Although the major sources of elements could be determined based on some important tracers (e.g., K, V), the contributions of major sources to each element still remained unknown. Therefore, Positive matrix factorization (PMF 5.0) version was applied to identify more source information of elements in $PM_{2.5}$ during 2017-2020 based on deweathered levels. After 20 runs, more than 26000 samples were trained to determine the optimal six factors with the lowest values of Q (robust) and Q (true). The BS, DISP, and BS-DISP methods confirmed that the most reliable solution was obtained with six factors. The detailed information of PMF analysis and error diagnostics are summarized in Table S4-6.

As shown in Figure S9, the trace elements in $PM_{2.5}$ during 2017-2020 showed similar cluster

characteristics. Factor 1 possesses high loadings of K (55%) and Se (42%). K and Se were often regarded as the major tracers of biomass burning. Due to the increasing usage of biomass fuels for domestic heating during the heating season, K and Se in $PM_{2.5}$ of Tangshan showed the higher values in winter, suggesting that these metals in fine particles could originate from the combustion of biomass fuels. Except the domestic heating, we found some episodes during harvesting season in late summer (2450 and 11.2 ng/m^3) and early autumn (2630 and 9.5 ng/m^3) also showed extremely high concentrations of K, which might be linked with local biomass burning (Chen et al., 2017). Based on the map of fire points and backward air masses trajectories (Figure S6-8), the metals released from biomass burning in NCP could be transported to the sampling site by the dominant southerly wind, which further proved the impacts of biomass burning (Chen et al., 2017).

The abundant elements in factor 2 included Ag (53%), Zn (51%), and Cu (36%). Owing to the higher temperatures during the roasting, sintering and smelting processes for the extraction of Cu, and Zn from ores, some metals such Ag in nonferrous metal ores could be vaporized as the byproduct and released into the flue gas (Pacyna and Pacyna, 2001; Wu et al., 2012). Therefore, the factor 2 was interpreted as the non-ferrous metal smelting source.

Factor 3 was characterized by a large mass fraction of Co (81%), Pb (61%), Hg (57%), and As (39%). After the phase-out of leaded gasoline since 1980s, the contribution from coal combustion to Pb suffered from rapid increase and accounted for the major fraction of particulate Pb (Das et al., 2018). Meanwhile, Co and Hg were also treated as the important byproducts released from coal burning and the Co and Hg concentrations often increased significantly with the elevation of burning temperature (Tang et al., 2018). Tian et al. (2015) estimated that 73% of As, 56 % of Pb, and 47 % of Hg were found to be emitted from coal combustion in China. Coal consumption in South China was mainly driven by coal-fired power plants, while the coal-based heating was the major sector for the coal consumption in NCP. In our study, As, Co and Pb showed the higher concentrations in winter (heating season) (18.7, 0.9, and 76 ng/m^3) compared with other seasons (14, 0.6, and 51 ng/m^3). The markedly seasonal discrepancies of As, Co and Pb strongly supported the impact of the coal combustion for domestic heating on the enhancement of As, Co and Pb in the fine particles.

Factor 4 was distinguished by high loadings of Cr (78%) and Mn (39%), respectively. Cr and Mn were mainly sourced from metallurgical industry such as steel production and ferrous metal

smelting (Liu et al., 2018a; Tian et al., 2015; Zhu et al., 2018). China occupied more than 49% of world steel production in 2017 (approximate 830 million tons), and 60% large steel producers were located in China (Chang et al., 2018). Tangshan possesses many large steel production industries such as Tangshan Steel, Qian'an Steel, and Guofeng Steel. Besides, some industries of Capital Steel have been migrated into Tangshan (Li et al., 2019), which might increase the Cr and Mn emissions.

Factor 5 explained 10.1% of the total species and it was characterized by high loadings of V (88%) and Ni (51%). It was well documented that V was a key fingerprint of heavy oil combustion, which was generally emitted from shipping emission and petrochemical refining (Shafer et al., 2012). However, Ni was widely utilized as a tracer of fuel oil combustion in industries (Zhu et al., 2018). Many oil-fired power plants were located in Tangshan for central heating (Yu et al., 2013). Based on the backward trajectory and wind direction (Figure S6-S8), we found that high concentrations of V and Ni might be derived from the southeastern air masses especially in summer and autumn, indicating the impacts of coastal port and petroleum refinery industry. In addition, both of V and Ni concentrations displayed the gradual decreases along the Southeast-Northwest transect, indicating the potential sources were located on Southeast Tangshan (Figure S8). Gathering evidence suggested that the V/Ni ratio in petroleum coke with a low-sulfur content and fuel oil usage ranged from 1 to 3 (Moreno et al., 2010). The annual mean ratios of V and Ni in our study reached 1.2 during the sampling period, which was in the range of this interval. The result also revealed that petrochemical refining and heavy oil combustion derived from coastal shipping emission might be an important source of V and Ni the fine particles.

Factor 6 was characterized by high loadings of Ca (78%), Cu (32%), and Fe (33%), and moderate loadings of Mn (31%) and Zn (29%). Some previous studies have demonstrated that both of Cu, Fe, and Zn were released from tyre and brake wear because they were the necessary materials for brake pads and the agents in brake linings (Dall'Osto et al., 2013; Hjortenkrans et al., 2007). Ca was probably sourced from the road fugitive dust because it was one of the most abundant elements in the upper continents (Alves et al., 2015; Liu et al., 2018a). Moreover, we have found Fe, Ca, and Zn displayed remarkably high values during the morning rush hours and a small peak during the sunset (Figure S10), which was coincident to the diurnal variation of traffic volume. Thus, the factor 6 was identified as the traffic-related dust source.

Although six similar sources were revealed during 2017-2020, the contribution concentrations and ratios of these sources varied greatly in these years. As shown in Figure 7 and 8, the contribution concentrations of biomass burning, non-ferrous metal smelting, coal combustion, and ferrous metal smelting to trace elements decreased from 1458, 479, 636, and 569 ng/m^3 to 901, 225, 230, and 345 ng/m^3, respectively. However, the contribution concentrations of heavy oil combustion and traffic-related dust displayed slight increase during 2017-2019, while they decreased rapidly after 2019. The contribution concentrations for nearly all of the sources to trace elements suffered from decreases during 2017-2020 because the total deweathered levels of trace elements experienced decreases in the past three years. However, the contribution ratios of these sources to trace elements did not show similar characteristics. For instance, the contribution ratio of traffic-related dust increased from 25% to 33%. However, the contributions of non-ferrous metal smelting and coal combustion decreased from 11% to 8% and 15% to 8%, respectively. The contributions of ferrous metal smelting, heavy oil combustion, and biomass burning remained relatively stable during this period.

Due to the strict implementation of clean air policy, many outdated industrial capacities were shut down and the cleaner technologies have been upgraded, which facilitated the production decreases of pig iron and coal-fired power plants (Ma et al., 2019). Hence, the contribution concentrations and ratios of non-ferrous metal smelting and coal combustion experienced dramatic decreases. Although the open biomass burning has been strictly restricted in Tangshan (Chang et al., 2018), the contribution ratios of biomass burning to trace elements in $PM_{2.5}$ remained relatively stable, which might be attributable to the rapid decreases of the contributions derived from coal combustion and non-ferrous metal smelting. In addition, the biofuel combustion was still widespread in some rural and suburb areas (Kamal et al., 2015; Li et al., 2020), which might offset the decreases in the contributions of open biomass burning. Although the contribution concentrations of traffic-related dust to trace elements also showed slight decrease, the contribution ratios of traffic-related dust to some trace elements exhibited the marked increases (8%) during 2017-2020 because the contribution ratios of metal smelting and coal combustion suffered from substantial decreases. The result also demonstrated that the implementation of coal to gas project facilitated the decreases of trace element concentrations. In addition, the source variation trend also suggested that the

formulation of many new quality standards for non-road diesel fuels cannot fully decrease the element emissions (Cui et al., 2017), and thus the control of traffic-related dust should be enhanced in the future.

3.5 Health risk assessment of trace metals in $PM_{2.5}$

Although the trace metals only accounted for minor fraction of total mass concentration of $PM_{2.5}$, it might pose a great threaten to the human health because most of these metals were bioavailable and non-degradable (Rai et al., 2019; Yi et al., 2011). Unfortunately, previous studies mainly used the filter sampling techniques to determine the concentrations of trace metals and then assess their health risks (Cui et al., 2018; Huang et al., 2016). These low-resolution data might not accurately reflect the real health risks triggered by metal exposure. In our study, we employed the online data to assess the health risks derived from metal exposure.

The health risks of trace metals could be classified into two types including carcinogenic and non-carcinogenic risk. Based on the major parameters summarized in Table S7 and Table S8, we estimated both of the carcinogenic and non-carcinogenic risks of major metals. To evaluate the impacts of emission control measures on element concentrations, both of the health risks based on original element levels and deweathered element concentrations were calculated. The mean CR values based on original concentrations were in the order of Pb (2.3×10^{-6} (adult) and 1.4×10^{-6} (child)) > As (1.9×10^{-6} and 1.1×10^{-6}) > Cr (0.11×10^{-6} and 0.07×10^{-6}). The total CR values for adults and children reached 4.3×10^{-6} and 2.6×10^{-6} (Table 2), respectively. The total CR values were located in the range of the acceptable (10^{-6}) and least stringent risk levels (10^{-4}), which suggested that Tangshan suffered from slight metal carcinogenic risk. Among all of these metals, Pb and As displayed the higher CR values. It was assumed that the coal combustion for domestic heating might be the dominant factor for the higher risks of Pb and As in Tangshan because both of Pb and As in $PM_{2.5}$ were mainly derived from coal combustion. With regard to the non-carcinogenic risks of trace metals, the HQ of As (1.2×10^{-2} and 2.9×10^{-2}) and Pb (6.8×10^{-4} and 17×10^{-4}) showed the higher values compared with other elements. The result indicated that nearly all of the elements did not display potential non-carcinogenic risk because HQ values of all the metals were less than 1. The total HQ value of these metals were also lower than 1, indicating that the trace elements in Tangshan did not show significant non-carcinogenic risk.

By removing the impact of meteorological conditions, we can isolate the impact of clean air policy on health risks associated with metal exposure alone. The decrease ratios of CR values based on the deweathered As and Pb concentrations during 2017-2020 were 54% and 62%, respectively (Table 3). However, the decrease ratios of CR values based on original As and Pb levels only reached 44%. The result suggested that the clean air policy in recent years significantly decreased the As and Pb emissions. Additionally, the decrease ratios of HQ values for original Cu (41%) and Zn (53%) were much less than those for deweathered ones (Cu: 47% and Zn: 59%). Nevertheless, some other elements did not show the similar characteristics. For instance, the decrease ratios of HQ values for original Cr (21%) and Fe (27%) were even slightly higher than those for deweathered ones (Cr: 19% and Fe: 23%). It was assumed that the clean air policy in recent years facilitated the emission reduction of non-ferrous metal smelting and coal combustion efficiently. However, the concentrations of elements derived from ferrous metal smelting and vehicle emission did not show marked decreases, which was in good agreement with the source apportionment result in the section 3.3. Thus, in the future work, it is highly imperative to further reduce the industrial/traffic-related emissions in order to alleviate potential health risks.

3.6 Limitations and uncertainties

It should be noted that our work is still subject to some limitations. At first, some elements such as Cr (0.5) and Ga (0.5) showed relatively lower CV R^2 values though they were generally higher than 0.5. These elements might show the higher uncertainties during the meteorology-normalization compared with other elements such as Cu (0.85) and K (0.85). Besides, few variables were applied to deweather the element concentrations, which might be responsible for the lower CV R^2 value for some elements. Due to the lack of available hourly emission inventory of each element, we only used the time variable to train the model. This method still suffered from some uncertainties, which should be improved by the establishment of near-time emission database.

4. Conclusions and implications

Three-year continuous hourly observation of elements in $PM_{2.5}$ was conducted in Tangshan during September 2017-August 2020. The effect of air clean policy on element concentrations in $PM_{2.5}$ were quantified. The main conclusions were drawn as follows:

(1) The deweathered concentrations of Ga, Co, Pb, Zn, and As showed the rapid decreases from

519 1.52 to 0.42 ng/m^3 (72%), 1.31 to 0.44 ng/m^3 (67%), 92 to 35 ng/m^3 (62%), 411 to 170 ng/m^3
520 (59%), and 21 to 10 ng/m^3 (54%), respectively. Clean air actions played the important role on
521 the emission reduction of coal combustion and non-ferrous metal smelting.
522 (2) The deweathered levels of Ca (8.3%), Cr (19%), and Fe (23%) displayed relatively low
523 decreases compared with other elements, indicating that the vehicle emission and ferrous-
524 smelting industries might be not sensitive to the air clean policy.
525 (3) The deweathered levels of some elements related with industrial activities (e.g., Ga, Zn, and Cr)
526 exhibited rapid decreases in autumn and winter compared with other seasons during 2017-2020,
527 while the combustion-related elements such as Pb and As did not show high decreasing ratios
528 in winter. The enhanced coal consumption during the heating season offset the benefits derived
529 from strict emission controls measures.
530 (4) The favorable meteorological conditions promoted the decreases of Ca (-25%), V (-10%), Cr (-
531 2.6%), Mn (-0.68%), Fe (-4.6%), Ni (-7.6%), and Cu (-21%) concentrations.
532 (5) The contribution ratios of biomass burning, non-ferrous metal smelting, coal combustion,
533 ferrous metal smelting, heavy oil combustion, and traffic-related dust changed from 33%, 11%,
534 15%, 13%, 3%, and 25% to 33%, 8%, 8%, 13%, 4%, and 33%, respectively.
535 (6) All of the elements did not show significant noncarcinogenic and carcinogenic risks, while both
536 of As and Pb still displayed relatively high health damages.
537 Our study presented detailed information about the impact of clean air policy on the chemical
538 compositions and source apportionment of trace elements in $PM_{2.5}$ in Tangshan, and provided new
539 enlightenment for scientific community and policymakers. Many targeted measures could be
540 undertaken to alleviate the air pollution and further to reduce avoided premature health risks.
541 However, this study still suffered some limitations and more steps will be taken toward thoroughly
542 addressing these problems. First of all, the PMF model still showed some uncertainties, and thus
543 characterizing the isotopic signatures of these elements is of great significance. In addition, Sunset
544 OC/EC analyzer, Monitoring of Aerosols and Gases (MARGA) platform, and other on-line
545 measurements should be collocated to probe into the synergistic effect of emission reduction and
546 meteorology on air quality.
547 **Acknowledgements**

This work was supported by the National Natural Science Foundation of China (42107113).

Data availability

The boundary layer height dataset was obtained from the website of https://www.ecmwf.int/. The dataset is archived in https://zenodo.org/record/7031975#.Ywys8cjfmfU (Li et al., 2022).

Author contributions

LR wrote the manuscript. LR, PM, ZWD, and HJM contributed to the conceptualization of the study. LR and PM conducted the research, and visualized the results. WGH revised the manuscript.

Competing interests

The contact author has declared that neither they nor their co-authors have any competing interests.

References

D'Alessandro, A., Lucarelli, F., Mandò, P.A., Marcazzan, G., Nava, S., Prati, P., Valli, G., Vecchi, R., Zucchiatti, A.: Hourly elemental composition and sources identification of fine and coarse PM10 particulate matter in four Italian towns. J. Aero. Sci., 34, 243-259, 2003.

Alies, B., Sasaki, I., Proux, O., Sayen, S., Guillon, E., Faller, P., and Hureau, C.: Zn impacts Cu coordination to amyloid-β, the Alzheimer's peptide, but not the ROS production and the associated cell toxicity. Chem. Commun., 49, 1214-1216, 2013.

Alves, C., Gomes, J., Nunes, T., Duarte, M., Calvo, A.I., Custodio, D., Pio, C., Karanasiou, A., and Querol, X.: Size-segregated particulate matter and gaseous emissions from motor vehicles in a road tunnel. Atmos. Res., 153, 134-144, https://doi.org/10.1016/j.atmosres.2014.08.002, 2015.

Ao, M., Qiu, G., Zhang, C., Xu, X., Zhao, L., Feng, X., Qin, S., and Meng, B.: Atmospheric deposition of antimony in a typical mercury-antimony mining area, Shaanxi Province, Southwest China. Environ. Pollut., 245, 173-182, https://doi.org/10.1016/j.envpol.2018.10.125, 2019.

Chang, Y., Huang, K., Xie, M., Deng, C., Zou, Z., Liu, S., and Zhang, Y.: First long-term and near real-time measurement of trace elements in China's urban atmosphere: temporal variability, source apportionment and precipitation effect. Atmos. Chem. Phys., 18, 11793-11812, https://doi.org/10.5194/acp-18-11793-2018, 2018.

Chen, J., Li, C., Ristovski, Z., Milic, A., Gu, Y., Islam, M.S., Wang, S., Hao, J., Zhang, H., and He, C.: A review of biomass burning: Emissions and impacts on air quality, health and climate in China. Sci. Total Environ., 579, 1000-1034, https://doi.org/10.1016/j.scitotenv.2016.11.025, 2017.

Chen, G.B., Li, S.S., Knibbs, L.D., Hamm, N.A.S., Cao, W., Li, T.T., Guo, J.P., Ren, H.Y., Abramson, M.J., and Guo, Y.M.: A machine learning method to estimate $PM_{2.5}$ concentrations across China with remote sensing, meteorological and land use information. Sci. Total Environ., 636, 52-60, https://doi.org/10.1016/j.scitotenv.2018.04.251, 2018.

Clements, A.L., Buzcuguven, B., Fraser, M.P., Kulkarni, P., and Chellam, S.: Role of particulate metals in heterogenous secondary sulfate formation. Atmos. Environ., 75, 233-240, https://doi.org/10.1016/j.atmosenv.2013.04.038, 2013.

Clements, N., Eav, J., Xie, M., Hannigan, M. P., Miller, S. L., Navidi, W., et al.: Concentrations and source insights for traceelements infine and coarse particulate matter. Atmospheric Environment,89, 373–381, https://doi.org/10.1016/j.atmosenv.2014.01.011, 2014.

Cui, L., Duo, B., Zhang, F., Li, C., Fu, H., and Chen, J.: Physiochemical characteristics of aerosol particles collected from the Jokhang Temple indoors and the implication to human exposure. Environ. Pollut., 236, 992-1003, https://doi.org/10.1016/j.envpol.2017.10.107, 2018.

Cui, M., Chen, Y., Feng, Y., Li, C., Zheng, J., Tian, C., Yan, C., and Zheng, M.: Measurement of PM and its chemical composition in real-world emissions from non-road and on-road diesel vehicles. Atmos. Chem. Phys., 17, 6779-6795, https://doi.org/10.5194/acp-17-6779-2017, 2017.

Cui, X., Wang, X., and Liu, B.: The characteristics of heavy metal pollution in surface dust in Tangshan, a heavily industrialized city in North China, and an assessment of associated health risks. J. Geochem. Explor., 210, 106432, 2020.

Cui, Y., Ji, D., Chen, H., Gao, M., Maenhaut, W., He, J., and Wang, Y.: Characteristics and sources of hourly trace elements in airborne fine particles in urban Beijing, China. J. Geophys. Res. Atmos., 124, 11595-11613, https://doi.org/10.1029/2019JD030881, 2019.

Dall'Osto, M., Querol, X., Amato, F., Karanasiou, A., Lucarelli, F., Nava, S., Calzolai, G., and Chiari,

M.: Hourly elemental concentrations in $PM_{2.5}$ aerosols sampled simultaneously at urban background and road site during SAPUSS -diurnal variations and PMF receptor modelling. Atmos. Chem. Phys., 13, 4375-4392, 2013.

Das, R., Mohtar, A.T.B.M., Rakshit, D., Shome, D., and Wang, X.: Sources of atmospheric lead (Pb) in and around an Indian megacity. Atmos. Environ., 193, 57-65, https://doi.org/10.1016/j.atmosenv.2018.08.062, 2018.

Duan, J. and Tan, J.: Atmospheric heavy metals and arsenic in China: situation, sources and control policies. Atmos. Environ., 74, 93-101, 10.1016/j.atmosenv.2013.03.031, 2013.

Fang, B., Zhang, L., Zeng, H., Liu, J., Yang, Z., Wang, H., Wang, Q., and Wang, M.: $PM_{2.5}$-bound polycyclic aromatic hydrocarbons: sources and health risk during non-heating and heating periods (Tangshan, China). Int. J. Env. Res. Pub. He., 17, 483, 2020.

Fernandez, J.A., Rey, A., and Carballeira, A.: An extended study of heavy metal deposition in Galicia (NW Spain) based on moss analysis. Sci. Total Environ., 254, 31-44, 10.1016/s0048-9697(00)00431-9, 2000.

Furger, M., Minguillon, M.C., Yadav, V., Slowik, J.G., Huglin, C., Frohlich, R., Petterson, K., Baltensperger, U., and Prevot, A.S.H.: Elemental composition of ambient aerosols measured with high temporal resolution using an online XRF spectrometer. Atmos. Meas. Technol., 10, 2061-2076, https://doi.org/10.5194/amt-10-2061-2017, 2017.

Geng, G., Xiao, Q., Zheng, Y., Tong, D., Zhang, Y., Zhang, X., Zhang, Q., He, K., and Liu, Y.: Impact of China's air pollution prevention and control action plan on $PM_{2.5}$ chemical composition over eastern China. Sci. China Earth Sci., 62, 1872-1884, https://doi.org/10.1007/s11430-018-9353-x, 2019.

Grivas, G., Cheristanidis, S., Chaloulakou, A., Koutrakis, P., & Mihalopoulos, N.: Elemental composition and source apportionmentoffine and coarse particles at traffic and urban background locations in Athens, Greece.Aerosol and Air Quality Research,18, 1642–1659, 2018.

Guo, J., Tilgner, A., Yeung, C., Wang, Z., Louie, P.K.K., Luk, C.W.Y., Xu, Z., Yuan, C., Gao, Y., and Poon, S.: Atmospheric peroxides in a polluted subtropical environment: seasonal variation, sources and sinks, and importance of heterogeneous processes. Environ. Sci. Technol., 48, 1443-1450, https://doi.org/10.1021/es403229x, 2014.

Harmens, H., Norris, D.A., Steinnes, E., Kubin, E., Piispanen, J., Alber, R., Aleksiayenak, Y., Blum, O., Coskun, M., and Dam, M.: Mosses as biomonitors of atmospheric heavy metal deposition: Spatial patterns and temporal trends in Europe. Environ. Pollut., 158, 3144-3156, https://doi.org/10.1016/j.envpol.2010.06.039, 2010.

He, Q., Zhang, M., Song, Y., and Huang, B.: Spatiotemporal assessment of $PM_{2.5}$ concentrations and exposure in China from 2013 to 2017 using satellite-derived data. J. Cleaner Prod., 286, 124965, https://doi.org/10.1016/j.jclepro.2020.124965, 2021.

Hjortenkrans, D.S., Bergbäck, B.G., and Häggerud, A.V.: Metal emissions from brake linings and tires: case studies of Stockholm, Sweden 1995/1998 and 2005. Environ. Sci. Technol., 41, 5224-5230, https://doi.org/10.1021/es070198o, 2007.

Holden, P.A., Gardeatorresdey, J.L., Klaessig, F., Turco, R.F., Mortimer, M., Hundrinke, K., Hubal, E.A.C., Avery, D., Barcelo, D., and Behra, R.: Considerations of environmentally relevant test conditions for improved evaluation of ecological hazards of engineered nanomaterials. Environ. Sci. Technol., 50, 6124-6145, https://doi.org/10.1021/acs.est.6b00608, 2016.

Huang, C., Bao, L., Luo, P., Wang, Z., Li, S., and Zeng, E.Y.: Potential health risk for residents around a typical e-waste recycling zone via inhalation of size-fractionated particle-bound heavy metals. J

644 Hazard. Mater., 317, 449-456, 10.1016/j.jhazmat.2016.05.081, 2016.
645 Jeong, C., Wang, J.M., and Evans, G.J.: Source apportionment of urban particulate matter using hourly
646 resolved trace metals, organics, and inorganic aerosol components. Atmos. Chem. Phys., 1-32,
647 https://doi.org/10.5194/acp-2016-189, 2016.
648 Kamal, A., Cincinelli, A., Martellini, T., and Malik, R.N.: A review of PAH exposure from the combustion
649 of biomass fuel and their less surveyed effect on the blood parameters. Environ. Sci. Pollut. Res., 22,
650 4076-4098, 10.1007/s11356-014-3748-0, 2015.
651 Kang, S., Chen, P., Li, C., Liu, B., and Cong, Z.: Atmospheric aerosol elements over the inland Tibetan
652 Plateau: concentration, seasonality, and transport. Aerosol Air Qual. Res., 16, 789-800, 2016.
653 Ke, H.B., Gong, S.L., He, J.J., Zhou, C.H., Zhang, L., Zhou, Y.K.: Spatial and temporal distribution of
654 open bio-mass burning in China from 2013 to 2017. Atmospheric Environment., 210, 156-165, 2019.
655 Li, R., Fu, H., Cui, L., Li, J., Wu, Y., Meng, Y., Wang, Y., and Chen, J.: The spatiotemporal variation and
656 key factors of SO_2 in 336 cities across China. J. Cleaner Prod., 210, 602-611,
657 https://doi.org/10.1016/j.jclepro.2018.11.062, 2019.
658 Li, R., Zhao, Y., Fu, H., Chen, J., Peng, M., and Wang, C.: Substantial changes in gaseous pollutants and
659 chemical compositions in fine particles in the North China Plain during the COVID-19 lockdown
660 period: anthropogenic vs. meteorological influences. Atmos. Chem. Phys., 21, 8677-8692,
661 https://doi.org/10.5194/acp-21-8677-2021, 2021.
662 Li, R., Peng, M., Zhao, W.D., Wang, G.H., and Hao, J.M.: Data for "Measurement Report: Rapid changes
663 of chemical characteristics and health risks for high time-resolved trace elements in $PM_{2.5}$ in a typical
664 industrial city in response to stringent clean air actions", [dataset],
665 https://zenodo.org/record/7031975#.Ywys8cjfmfU, 2022.
666 Li, Z., Jiang, J., Ma, Z., Fajardo, O.A., Deng, J., and Duan, L.: Influence of flue gas desulfurization (FGD)
667 installations on emission characteristics of $PM_{2.5}$ from coal-fired power plants equipped with selective
668 catalytic reduction (SCR). Environ. Pollut., 230, 655-662,
669 https://doi.org/10.1016/j.envpol.2017.06.103, 2017.
670 Li, Z., Wang, Y., Li, Z., Guo, S., and Hu, Y.: Levels and sources of $PM_{2.5}$-associated pahs during and after
671 the wheat harvest in a central rural area of the beijing-tianjin-hebei (bth) region. Aerosol Air Qual.
672 Res., 20, 1070-1082, 2020.
673 Lin, Y., Hsu, S., Chou, C.C.K., Zhang, R., Wu, Y., Kao, S., Luo, L., Huang, C., Lin, S., and Huang, Y.:
674 Wintertime haze deterioration in Beijing by industrial pollution deduced from trace metal fingerprints
675 and enhanced health risk by heavy metals. Environ. Pollut., 208, 284-293,
676 https://doi.org/10.1016/j.envpol.2015.07.044, 2016.
677 Liu, H., He, K., Wang, Q., Huo, H., Lents, J., Davis, N., Nikkila, N., Chen, C., Osses, M., and He, C.:
678 Comparison of vehicle activity and emission inventory between Beijing and Shanghai. J. Air Waste
679 Manage., 57, 1172-1177, https://doi.org/10.3155/1047-3289.57.10.1172, 2007.
680 Liu, J., Chen, Y., Chao, S., Cao, H., Zhang, A., and Yang, Y.: Emission control priority of $PM_{2.5}$-bound
681 heavy metals in different seasons: A comprehensive analysis from health risk perspective. Sci. Total
682 Environ., 644, 20-30, https://doi.org/10.1016/j.scitotenv.2018.06.226, 2018a.
683 Liu, R., Men, C., Yu, W., Xu, F., Wang, Q., and Shen, Z.: Uncertainty in positive matrix factorization
684 solutions for PAHs in surface sediments of the Yangtze River Estuary in different seasons.
685 Chemosphere 191, 922-936, https://doi.org/10.1016/j.chemosphere.2017.10.070, 2018b.
686 Lopez-Cruz, J., Crespo-Salvador, O., Fernandez-Crespo, E., Garcia-Agustin, P., and Gonzalez-Bosch, C.:
687 Absence of Cu-Zn-superoxide dismutase BCSOD1 reduces Botrytis cinerea virulence in Arabidopsis

and in tomato plants, which reveals interplay among ROS, callose and signaling pathways. Mol. Plant Pathol., 18, 16-31, 2016.

Lyu, X.P., Chen, N., Guo, H., Zeng, L.W., Zhang, W.H., Shen, F., Quan, J.H., Wang, N.: Chemical characteristics and causes of airborne particulate pollution in warm seasons in Wuhan, central China. Atmos. Chem. Phys. 16, 10671–10687, www.atmos-chem-phys.net/16/10671/2016/, 2016

Lyu, Y., Zhang, K., Chai, F., Cheng, T., Yang, Q., Zheng, Z., and Li, X.: Atmospheric size-resolved trace elements in a city affected by non-ferrous metal smelting: Indications of respiratory deposition and health risk. Environ. Pollut., 224, 559-571, https://doi.org/10.1016/j.envpol.2017.02.039, 2017.

Ma, Z., Liu, R., Liu, Y., and Bi, J.: Effects of air pollution control policies on $PM_{2.5}$ pollution improvement in China from 2005 to 2017: a satellite-based perspective. Atmos. Chem. Phys., 19, 6861-6877, https://doi.org/10.5194/acp-19-6861-2019, 2019.

Manju, A., Kalaiselvi, K., Dhananjayan, V., Palanivel, M., Banupriya, G., Vidhya, M., Panjakumar, K., and Ravichandran, B.: Spatio-seasonal variation in ambient air pollutants and influence of meteorological factors in Coimbatore, southern India. Air Qual. Atmos. Heal., 11, 1179-1189, https://doi.org/10.1007/s11869-018-0617-x, 2018.

Manousakas, M., Papaefthymiou, H., Diapouli, E., Migliori, A., Karydas, A.G., Bogdanovic-Radovic, I., and Eleftheriadis, K.: Assessment of $PM_{2.5}$ sources and their corresponding level of uncertainty in a coastal urban area using EPA PMF 5.0 enhanced diagnostics. Sci. Total Environ. 574, 155-164, 2017.

Micheline, G., Rachida, C., Celine, M., Gaby, K., Rachid, A., and Petru, J.: Levels of Pb, Cd, Hg and As in fishery products from the eastern Mediterranean and human health risk assessment due to their Consumption. Interna. J. Environ. Res., 13, 443-455, https://doi.org/10.1007/s41742-019-00185-w, 2019.

Moreno, T., Querol, X., Alastuey, A., La Rosa, J.D.D., La Campa, A.M.S.D., Minguillon, M., Pandolfi, M., Gonzalez-Castanedo, Y., Monfort, E., and Gibbons, W.: Variations in vanadium, nickel and lanthanoid element concentrations in urban air. Sci. Total Environ., 408, 4569-4579, https://doi.org/10.1016/j.scitotenv.2010.06.016, 2010.

Oldani, K.M., Mladenov, N., Williams, M., Campbell, C.M., and Lipson, D.A.: Seasonal patterns of dry deposition at a high-elevation site in the colorado rocky mountains. J. Geophys. Res. Atmos., 122, 2017.

Olujimi, O.O., Oputu, O., Fatoki, O.S., Opatoyinbo, O.E., Aroyewun, O.A., and Baruani, J.: Heavy metals speciation and human health risk assessment at an illegal gold mining site in Igun, Osun State, Nigeria. J. Health. Pollut., 5, 19-32, 2015.

Paatero, P. and Tapper, U.: Positive matrix factorization: A non-negative factor model with optimal utilization of error estimates of data values. Environmetrics 5, 111-126, 1994.

Pacyna, J.M. and Pacyna, E.G.: An assessment of global and regional emissions of trace metals to the atmosphere from anthropogenic sources worldwide. Environ. Rev., 9, 269-298, 2001.

Prati, P., Zucchiatti, A., Lucarelli, F., Mandò, P.A.: Source apportionment near a steel plant in Genoa (Italy) by continuous aerosol sampling and PIXE analysis. Atmos. Environ., 34, 3149-3157, 2000.

Rai, P.K., Lee, S.S., Zhang, M., Tsang, Y.F., and Kim, K.: Heavy metals in food crops: Health risks, fate, mechanisms, and management. Environ. Interna., 125, 365-385, 2019.

Rasmussen, P.E.: Long-range atmospheric transport of trace metals: the need for geoscience perspectives. Environ. Earth Sci., 33, 96-108, 1998.

Reff, A., Eberly, S.I., and Bhave, P.V.: Receptor modeling of ambient particulate matter data using positive matrix factorization: review of existing methods. J. Air Waste Manage., 57, 146-154, 2007.

Ren, Z., Zhang, B., Lu, P., Li, C., Gao, L., and Zheng, M.: Characteristics of air pollution by polychlorinated dibenzo-p-dioxins and dibenzofurans in the typical industrial areas of Tangshan City, China. J. Environ. Sci. -China, 23, 228-235, 2011.

Saffari, A., Daher, N., Shafer, M.M., Schauer, J.J., and Sioutas, C.: Global perspective on the oxidative potential of airborne particulate matter: a synthesis of research findings. Environ. Sci. Technol., 48, 7576-7583, 2014.

Shafer, M.M., Toner, B.M., Overdier, J.T., Schauer, J.J., Fakra, S.C., Hu, S., Herner, J.D., and Ayala, A.: Chemical speciation of vanadium in particulate matter emitted from diesel vehicles and urban atmospheric aerosols. Environ. Sci. Technol., 46, 189-195, 2012.

Shi, G., Teng, J., Ma, H., Li, Y., and Sun, B.: Metals and metalloids in precipitation collected during CHINARE campaign from Shanghai, China, to Zhongshan Station, Antarctica: Spatial variability and source identification. Global Biogeochem. Cyc., 29, 760-774, 2015.

Storelli, M.M.: Potential human health risks from metals (Hg, Cd, and Pb) and polychlorinated biphenyls (PCBs) via seafood consumption : estimation of target hazard quotients (THQs) and toxic equivalents (TEQs). Food and Chemical Toxicology 46, 2782-2788, 2008.

Taghvaee, S., Sowlat, M.H., Mousavi, A., Hassanvand, M.S., Yunesian, M., Naddafi, K., and Sioutas, C.: Source apportionment of ambient $PM_{2.5}$ in two locations in central Tehran using the Positive Matrix Factorization (PMF) model. Sci. Total Environ., 628-629, 672-686, 2018.

Tang, Q., Sheng, W., Li, L., Zheng, L., Miao, C., and Sun, R.: Alteration behavior of mineral structure and hazardous elements during combustion of coal from a power plant at Huainan, Anhui, China. Environ. Pollut., 239, 768-776, 2018.

Tian, H., Zhu, C., Gao, J., Cheng, K., Hao, J., Wang, K., Hua, S., Wang, Y., and Zhou, J.: Quantitative assessment of atmospheric emissions of toxic heavy metals from anthropogenic sources in China: historical trend, spatial distribution, uncertainties, and control policies. Atmos. Chem. Phys., 15, 10127-10147, 2015.

Tianxue, W., Yuesi, W., Shihyu, C., and Guangren, L.: On-line measurement of water-soluble ions in ambient particles. Adv. Atmos. Sci., 23, 586-592, 2006.

Wang, S., Su, H., Chen, C., Tao, W., Streets, D.G., Lu, Z., Zheng, B., Carmichael, G.R., Lelieveld, J., and Pöschl, U.: Natural gas shortages during the "coal-to-gas" transition in China have caused a large redistribution of air pollution in winter 2017. P. Natl. Acad. Sci. USA, 117, 31018-31025, 2020a.

Wang, S., Su, H., Chen, C., Tao, W., Streets, D.G., Lu, Z., Zheng, B., Carmichael, G.R., Lelieveld, J., Pöschl, U., and Cheng, Y.: Natural gas shortages during the "coal-to-gas" transition in China have caused a large redistribution of air pollution in winter 2017. P. Natl. Acad. Sci. USA, 117, 31018-31025, 2020b.

Westerdahl, D., Wang, X., Pan, X., and Zhang, K.M.: Characterization of on-road vehicle emission factors and microenvironmental air quality in Beijing, China. Atmos. Environ., 43, 697-705, https://doi.org/10.1016/j.atmosenv.2008.09.042, 2009.

Witt, M.L.I., Baker, A.R., and Jickells, T.D.: Atmospheric trace metals over the Atlantic and South Indian Oceans: Investigation of metal concentrations and lead isotope ratios in coastal and remote marine aerosols. Atmos. Environ., 40, 5435-5451, https://doi.org/10.1016/j.atmosenv.2006.04.041, 2006.

Wu, Q., Wang, S., Zhang, L., Song, J., Yang, H., and Meng, Y.: Update of mercury emissions from China's primary zinc, lead and copper smelters, 2000-2010. Atmos. Chem. Phys., 12, 18207-18242, https://doi.org/10.5194/acp-12-11153-2012, 2012.

Wu, Y., Wang, R., Zhou, Y., Lin, B., Fu, L., He, K., and Hao, J.: On-road vehicle emission control in

776 beijing: past, present, and future. Environ. Sci. Technol., 45, 147-153,
777 https://doi.org/10.1021/es1014289, 2011.
778 Xiao, Q., Geng, G., Liang, F., Wang, X., Lv, Z., Lei, Y., Huang, X., Zhang, Q., Liu, Y., and He, K.:
779 Changes in spatial patterns of $PM_{2.5}$ pollution in China 2000-2018: Impact of clean air policies.
780 Environ. Interna., 141, 105776, https://doi.org/10.1016/j.envint.2020.105776, 2020.
781 Yang, Q., Yuan, Q., Li, T., Shen, H., and Zhang, L.: The relationships between $PM_{2.5}$ and meteorological
782 factors in China: seasonal and regional variations. Int. J. Env. Res. Pub. He., 14, 1510, 2017.
783 Yi, Y., Yang, Z., and Zhang, S.: Ecological risk assessment of heavy metals in sediment and human health
784 risk assessment of heavy metals in fishes in the middle and lower reaches of the Yangtze River basin.
785 Environ. Pollut., 159, 2575-2585, https://doi.org/10.1016/j.envpol.2011.06.011, 2011.
786 Yu, L., Wang, G., Zhang, R., Zhang, L., Song, Y., Wu, B., Li, X., An, K., and Chu, J.: Characterization
787 and source apportionment of $pm_{2.5}$ in an urban environment in beijing. Aerosol Air Qual. Res., 13,
788 574-583, doi: 10.4209/aaqr.2012.07.0192, 2013.
789 Song, Z.F.: An assessment of the heavy metal pollution and potential ecological hazards in urban soil of
790 Tangshan City. Geology in China 38, 1379-1386, 2011.
791 Zhang, J., Zhou, X., Wang, Z., Yang, L., Wang, J., Wang, W.: Trace elements in $PM_{2.5}$ in Shandong
792 Province: Source identification and health risk assessment. Science of the Total Environment 621,
793 558-577, 2018.
794 Zhang, Q., Zheng, Y., Tong, D., Shao, M., Wang, S., Zhang, Y., Xu, X., Wang, J., He, H., Liu, W., Ding,
795 Y., Lei, Y., Li, J., Wang, Z., Zhang, X., Wang, Y., Cheng, J., Liu, Y., Shi, Q., Yan, L., Geng, G., Hong,
796 C., Li, M., Liu, F., Zheng, B., Cao, J., Ding, A., Gao, J., Fu, Q., Huo, J., Liu, B., Liu, Z., Yang, F., He,
797 K., and Hao, J.: Drivers of improved $PM_{2.5}$ air quality in China from 2013 to 2017. P. Natl. Acad. Sci.
798 USA, 116, 24463-24469, https://doi.org/10.1073/pnas.1907956116, 2019.
799 Zhao, M., Zhang, Y., Ma, W., Fu, Q., Yang, X., Li, C., Zhou, B., Yu, Q., and Chen, L.: Characteristics
800 and ship traffic source identification of air pollutants in China's largest port. Atmos. Environ., 64, 277-
801 286, https://doi.org/10.1016/j.atmosenv.2012.10.007, 2013.
802 Zhu, C., Tian, H., Hao, Y., Gao, J., Hao, J., Wang, Y., Hua, S., Wang, K., and Liu, H.: A high-resolution
803 emission inventory of anthropogenic trace elements in Beijing-Tianjin-Hebei (BTH) region of China.
804 Atmos. Environ., 191, 452-462, https://doi.org/10.1016/j.atmosenv.2018.08.035, 2018.
805 Zhu, C., Tian, H., and Hao, J.: Global anthropogenic atmospheric emission inventory of twelve typical
806 hazardous trace elements, 1995–2012. Atmos. Environ., 220, 117061,
807 https://doi.org/10.1016/j.atmosenv.2019.117061, 2020.
808

Figure 1 The topographic map of China indicating the location of Tangshan (a), sampling site (b), and some major industrial points (b). The population distribution of Tangshan is also depicted in (b).

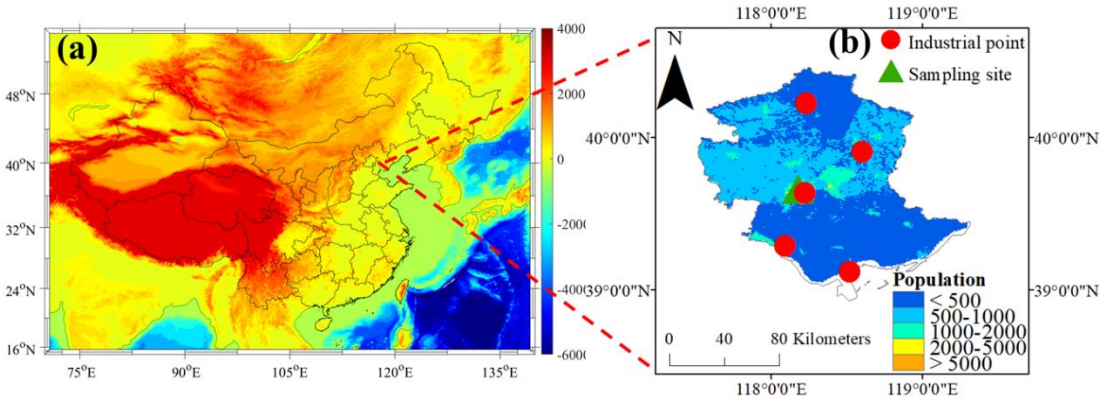

Figure 2 The bar chart of the concentrations of 16 trace elements including K, Fe, Ca, Zn, Pb, Mn, Fe, As, Se, V, Cr, Ag, Ni, Hg, Ga, and Co.

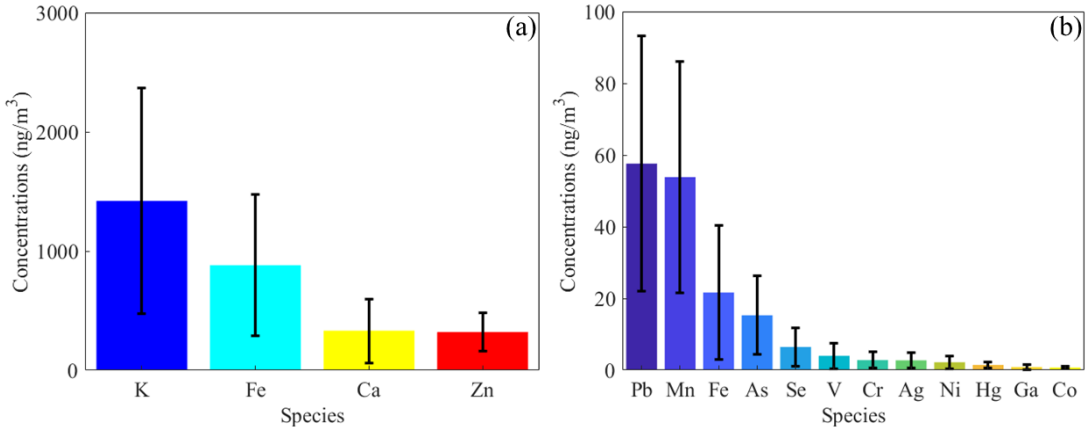

Figure 3 Inter-annual variations of original (red) and deweathered (manganese purple) element concentrations (ng/m^3) in $PM_{2.5}$ in Tangshan. The dark, nattier blue, and nattier yellow backgrounds represent the species during 2017-2018 (from September in 2017 to August in 2018), 2018-2019 (from September in 2018 to August in 2019), and 2019-2020 (from September in 2019 to August in 2020).

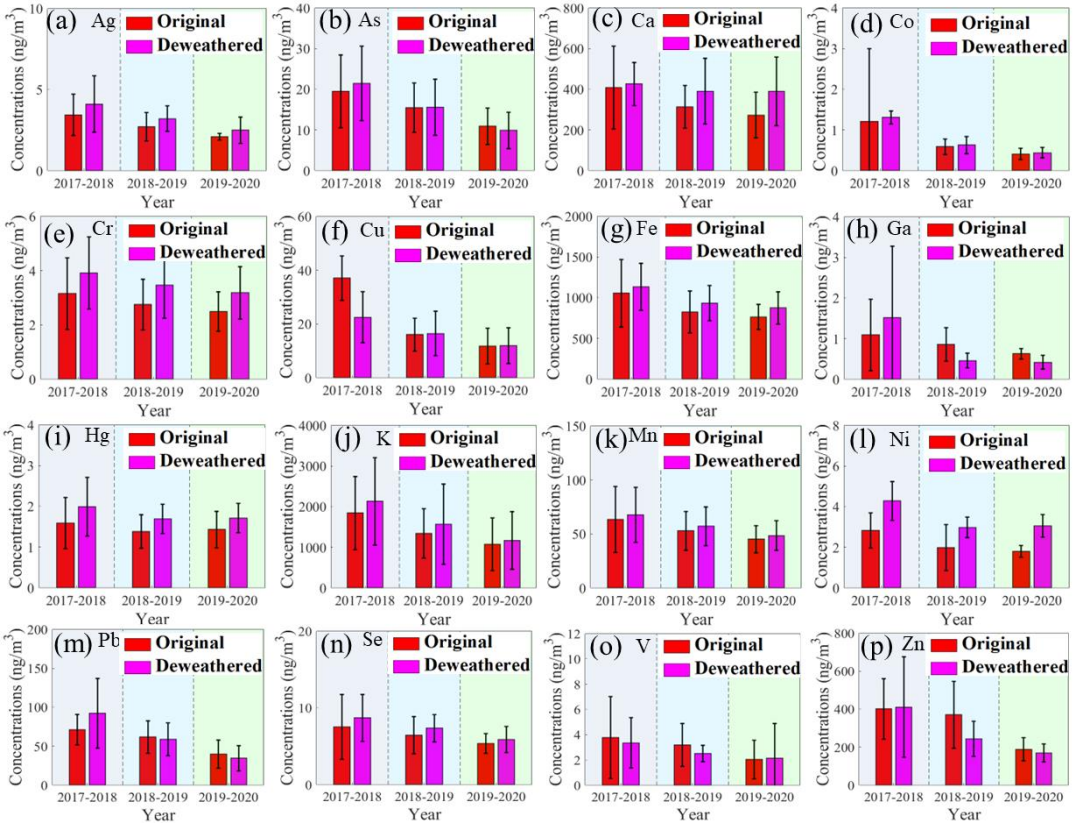

Figure 4 The original (red and orange) and deweathered (green and blue) element concentrations (ng/m^3) in $PM_{2.5}$ in Tangshan in four seasons during 2017-2018, 2018-2019, and 2019-2020. S1, U1, A1, and W1 represent the spring, summer, autumn, and winter during 2017-2018. S2, U2, A2, and W2 denote the spring, summer, autumn, and winter during 2018-2019. S3, U3, A3, and W3 are the spring, summer, autumn, and winter during 2019-2020.

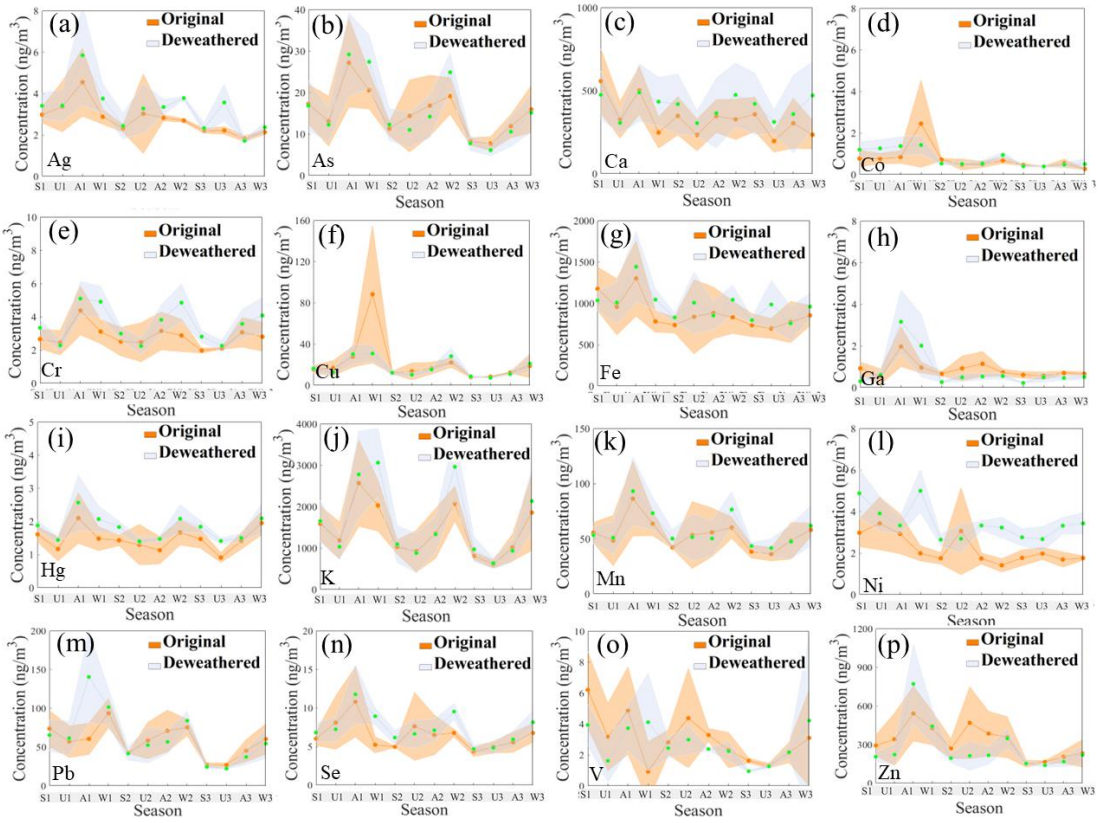

Figure 5 Weekly variations of original (green) and deweathered (orange) element concentrations (ng/m^3) in $PM_{2.5}$ in Tangshan. The green and dark backgrounds denote the error bars of original and deweathered elements, respectively.

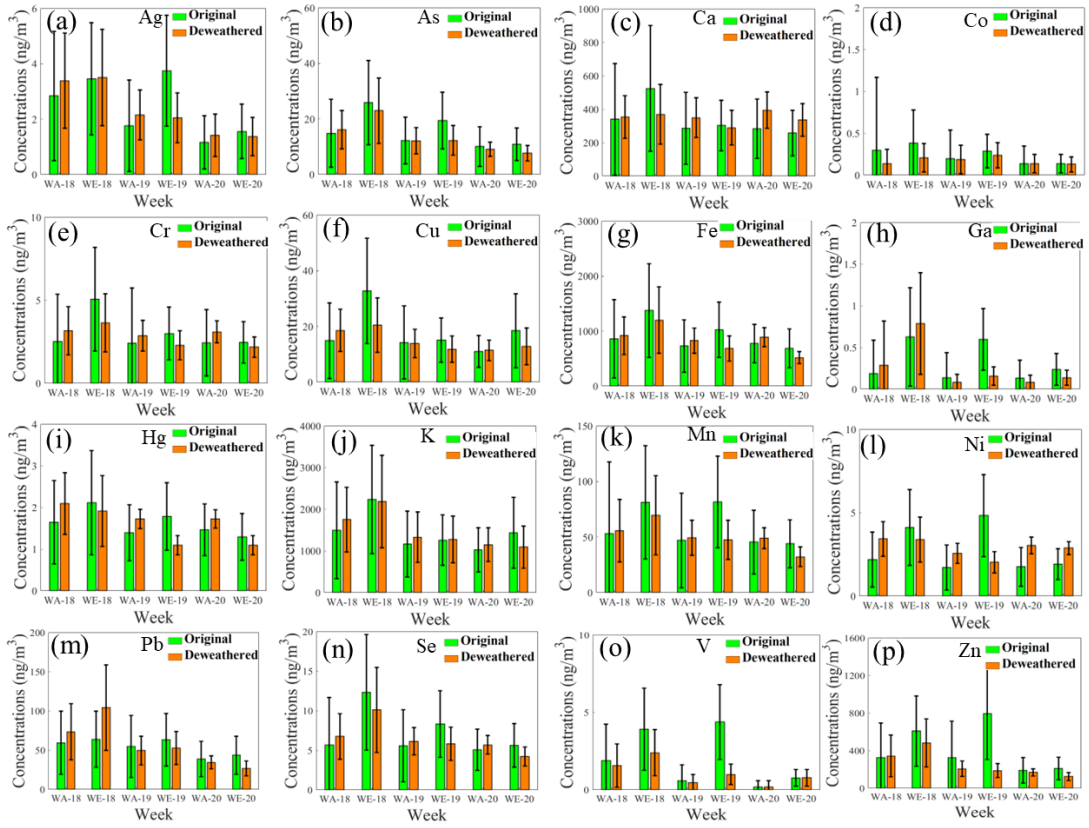

Figure 6 Relative importance of the predictors for the prediction of trace elements. The columns in the figure represent the variable importance in RF models for trace elements. P, RH, T, WD, WS, DOW, HOY, DOY, and Year denote air pressure, relative humidity, air temperature, wind direction, wind speed, day of week, hour of day, day of year, and study year, respectively.

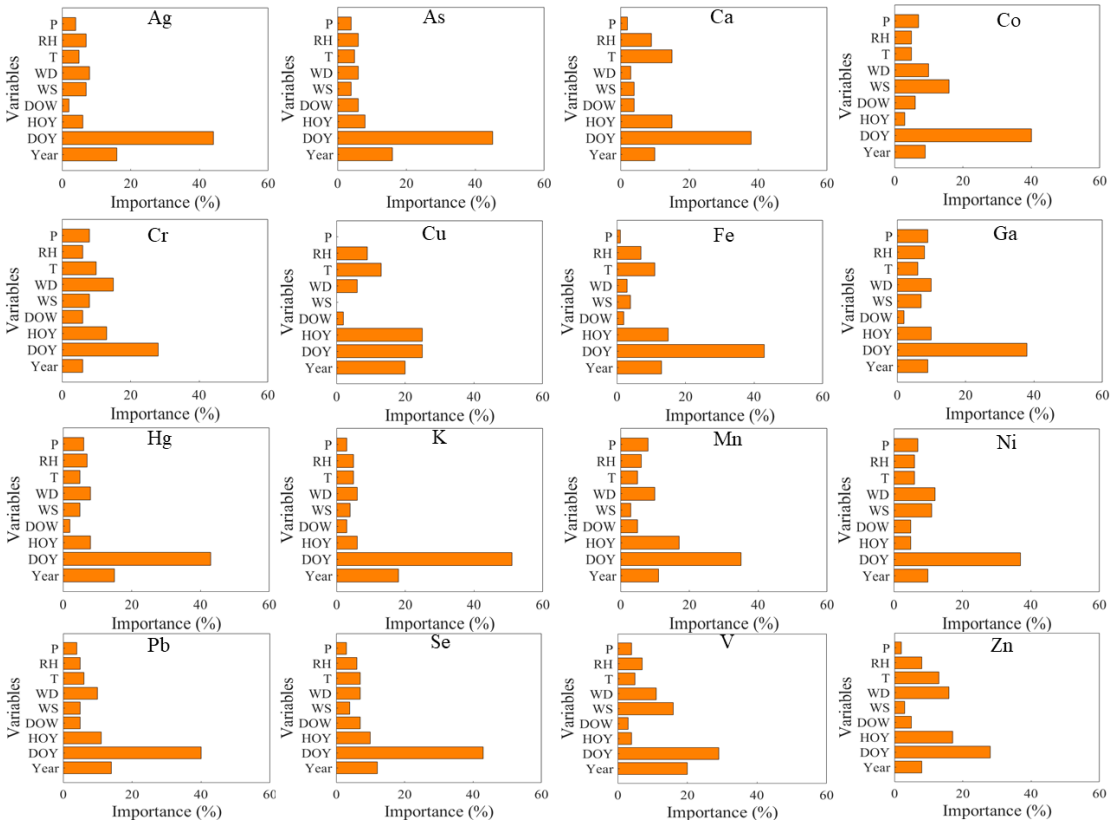

Figure 7 The deweathered concentrations of trace elements derived from six sources in Tangshan during 2017-2020.

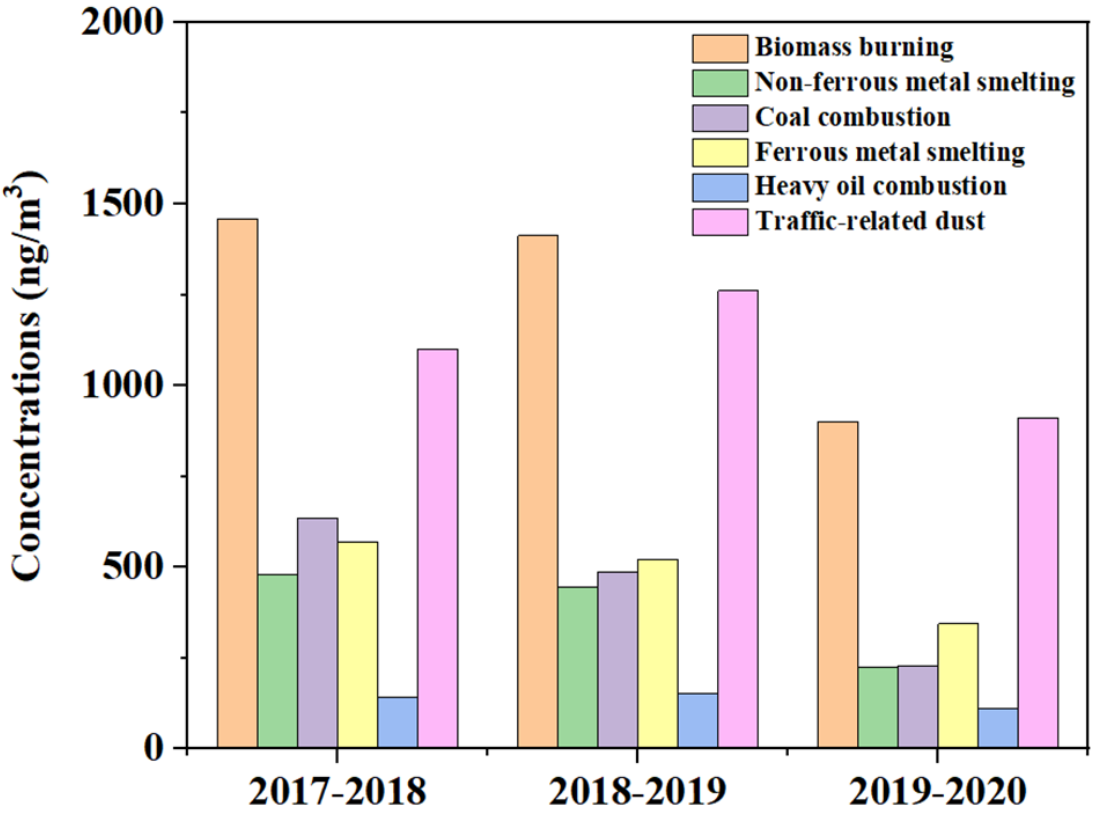

Figure 8 Average contributions of six sources to the deweathered concentrations of elements in $PM_{2.5}$ based on PMF model. The red panel means the biomass burning; the green panel denotes the non-ferrous metal smelting; the blue one represents the coal combustion; the cyan one is the ferrous metal smelting; the pink one represents the heavy oil combustion; and the yellow one denotes the traffic-related dust. (a), (b), and (c) represent the source contributions during 2017-2018, 2018-2019, and 2019-2020, respectively.

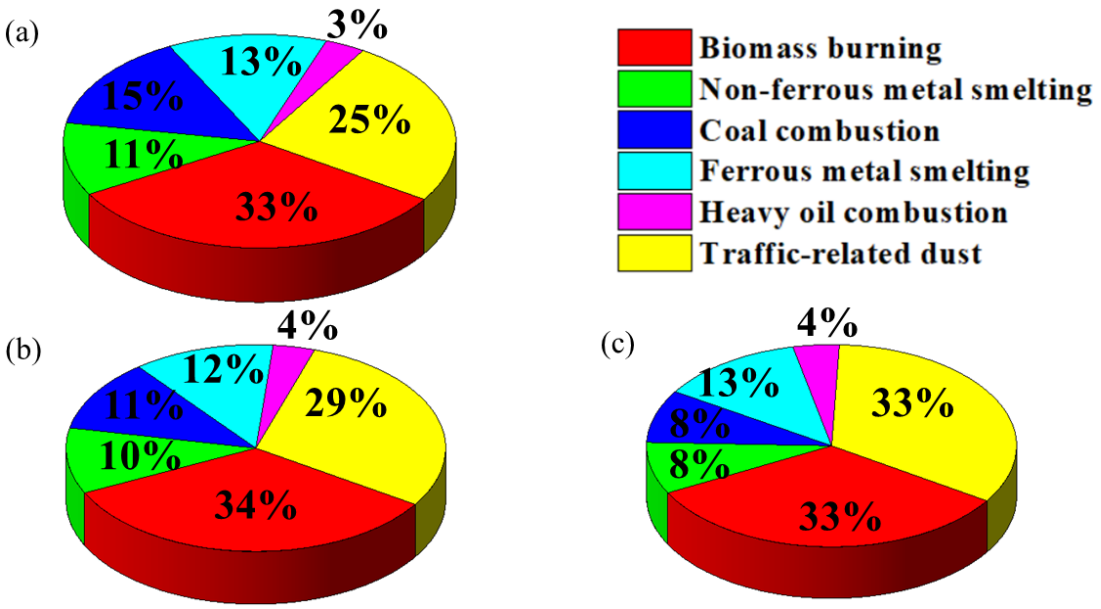

Table 1 The comparison of element concentrations in $PM_{2.5}$ of Tangshan and the standard values for these elements in World Health Organization (WHO), China, Europe, and the United States.

Elements	Mean±SD	CAAQS	WHO	EU	United States
Co	0.74±0.24				
Ga	0.86±0.74				
Hg	1.47±0.81	50	1000		
Ni	2.21±1.80		25	20	
Ag	2.75±2.08				
Cr	2.80±2.22	0.025	0.25		
V	3.98±3.57				
Se	6.46±5.28				
As	15.3±11.0	6	6.60	6	
Cu	21.7±18.7				
Mn	53.8±32.3				
Pb	57.6±35.7		1000		150
Zn	320±162				
Ca	332±268				
Fe	881 ± 591				
K	1421±947				

Table 2 The non-carcinogenic and carcinogenic risks for the original element levels in $PM_{2.5}$.

Age	Year	Indicator	Cr	Mn	Fe	Co	Ni	Cu	Zn	As	Pb
Adult	2017-2018	HQ	2.47×10^{-4}	1.07×10^{-4}	3.55×10^{-4}	4.50×10^{-4}	0.33×10^{-4}	1.18×10^{-4}	3.15×10^{-4}	1.53×10^{-2}	8.39×10^{-4}
		CR	0.13×10^{-6}	--	--	--	--	--	--	2.37×10^{-6}	2.88×10^{-6}
	2018-2019	HQ	2.16×10^{-4}	0.89×10^{-4}	2.77×10^{-4}	4.67×10^{-4}	0.23×10^{-4}	0.95×10^{-4}	2.91×10^{-4}	1.21×10^{-2}	7.28×10^{-4}
		CR	0.11×10^{-6}	--	--	--	--	--	--	1.87×10^{-6}	2.50×10^{-6}
	2019-2020	HQ	1.95×10^{-4}	0.76×10^{-4}	2.58×10^{-4}	3.26×10^{-4}	0.21×10^{-4}	0.70×10^{-4}	1.49×10^{-4}	0.86×10^{-2}	4.69×10^{-4}
		CR	0.10×10^{-6}	--	--	--	--	--	--	1.33×10^{-6}	1.61×10^{-6}
Child	2017-2018	HQ	6.02×10^{-4}	2.60×10^{-4}	8.64×10^{-4}	11.1×10^{-4}	0.81×10^{-4}	2.87×10^{-4}	7.67×10^{-4}	3.73×10^{-2}	20.4×10^{-4}
		CR	0.08×10^{-6}	--	--	--	--	--	--	1.44×10^{-6}	1.75×10^{-6}
	2018-2019	HQ	5.26×10^{-4}	2.17×10^{-4}	6.74×10^{-4}	11.0×10^{-4}	0.57×10^{-4}	2.30×10^{-4}	7.08×10^{-4}	2.95×10^{-2}	17.7×10^{-4}
		CR	0.07×10^{-6}	--	--	--	--	--	--	1.14×10^{-6}	1.52×10^{-6}

2019-2020	HQ	4.75×10^{-4}	1.85×10^{-4}	6.27×10^{-4}	7.93×10^{-4}	0.52×10^{-4}	1.70×10^{-4}	3.61×10^{-4}	2.09×10^{-2}	11.4×10^{-4}
	CR	0.06×10^{-6}	--	--	--	--	--	--	0.81×10^{-6}	0.98×10^{-6}

Table 3 The non-carcinogenic and carcinogenic risks for the deweathered element levels in $PM_{2.5}$.

Age	Year	Indicator	Cr	Mn	Fe	Co	Ni	Cu	Zn	As	Pb
Adult	2017-2018	HQ	3.07×10^{-4}	1.14×10^{-4}	3.82×10^{-4}	10.3×10^{-4}	0.50×10^{-4}	1.33×10^{-4}	3.15×10^{-4}	1.68×10^{-2}	10.8×10^{-4}
		CR	0.16×10^{-6}	--	--	--	--	--	--	2.60×10^{-6}	3.72×10^{-6}
	2018-2019	HQ	2.73×10^{-4}	0.96×10^{-4}	3.14×10^{-4}	4.93×10^{-4}	0.35×10^{-4}	0.97×10^{-4}	2.91×10^{-4}	1.22×10^{-2}	6.91×10^{-4}
		CR	0.14×10^{-6}	--	--	--	--	--	--	1.89×10^{-6}	2.37×10^{-6}
	2019-2020	HQ	2.50×10^{-4}	0.82×10^{-4}	2.95×10^{-4}	3.46×10^{-4}	0.36×10^{-4}	0.70×10^{-4}	1.49×10^{-4}	0.78×10^{-2}	4.08×10^{-4}
		CR	0.13×10^{-6}	--	--	--	--	--	--	1.20×10^{-6}	1.40×10^{-6}
Child	2017-2018	HQ	7.47×10^{-4}	2.77×10^{-4}	9.28×10^{-4}	11.7×10^{-4}	1.23×10^{-4}	3.22×10^{-4}	3.23×10^{-4}	4.09×10^{-2}	26.4×10^{-4}
		CR	0.10×10^{-6}	--	--	--	--	--	--	1.58×10^{-6}	2.26×10^{-6}
	2018-2019	HQ	6.64×10^{-4}	2.34×10^{-4}	7.64×10^{-4}	11.9×10^{-4}	0.85×10^{-4}	2.36×10^{-4}	1.91×10^{-4}	2.98×10^{-2}	16.8×10^{-4}
		CR	0.09×10^{-6}	--	--	--	--	--	--	1.15×10^{-6}	1.44×10^{-6}

2019-2020	HQ	6.08×10^{-4}	1.99×10^{-4}	7.17×10^{-4}	8.42×10^{-4}	0.87×10^{-4}	1.71×10^{-4}	1.34×10^{-4}	1.89×10^{-2}	9.92×10^{-4}
	CR	0.08×10^{-6}	--	--	--	--	--	--	0.73×10^{-6}	0.85×10^{-6}